

SPRINGING AND SLOW-DRIFT RESPONSES: PREDICTED EXTREMES AND FATIGUE VS. SIMULATION

Steven R. Winterstein¹, Todd C. Ude¹, and Gudmund Kleiven²

¹Civil Engineering Dept., Stanford University

²Norsk Hydro a.s; Visiting Scholar at Stanford University

ABSTRACT

This study addresses statistical analysis of second-order load and response models of large-volume structures, such as tension-leg platforms (TLPs). We show here a general statistical model that directly estimates both extremes and fatigue of these load and response motions. It can be applied directly to an arbitrary second-order model: sum- plus difference frequency, first- plus second-order response. Extensive time-domain simulations are performed for verification. Two TLP applications are considered: a springing example of tether tension and fatigue, and a slow-drift example of extreme surge motions.

KEYWORDS

Nonlinear diffraction; offshore structures; random vibration; springing; slow-drift; structural reliability; tension-leg platforms (TLPs).

INTRODUCTION

Second-order Volterra models have gained increasing use, to reflect both the non-Gaussian wave elevation process and the corresponding forces and motions of large-volume structures. Various computer codes are now available to estimate the required quadratic transfer functions from wave elevation to forces (e.g., Molin and Chen, 1990; WAMIT, 1991). As the ability to compute these quadratic transfer functions (QTFs) increases, so does the need to assess their practical consequences for engineering design; e.g., their effect on extreme response and fatigue damage.

Statistics of second-order models have been studied by various authors (e.g., Langley and McWilliam, 1993; Næss, 1987; Næss, 1989; Næss, 1992; Stansberg, 1991; Winterstein and Marthinssen, 1991). Such analyses are often restricted, however, to only the sum frequency (springing) or difference frequency (slow drift) response. In addition, first-order response contributions are often

excluded, or included only through an empirical load combination rule. Moreover, verification through simulation is often lacking.

Our goals here are twofold. First, we show a general statistical model—the Hermite model—that directly estimates extremes and fatigue. It can be applied directly to an arbitrary second-order model: sum- plus difference frequency, first- plus second-order response. Second, we perform extensive time-domain simulations for verification. Two tension-leg platform applications are considered: a springing example of tether tension and fatigue, and a slow-drift example of extreme surge motions.

The Hermite model achieves its generality by requiring only five response quantities: an average frequency and the first four statistical moments: mean, standard deviation, skewness, and kurtosis. These moments are conveniently calculated by eigenvalue analysis (Kac and Siebert, 1947). This analysis is summarized below, in a general formulation not specialized to the either sum- or difference-frequency case. Indeed, the same Hermite methodology can be applied to other nonlinearities (e.g., higher-order load mechanisms), provided the requisite four moments can be estimated from either theory or data.

The generality of the Hermite model does not come without cost. Its virtue is that only four moments are needed; its corresponding drawback is that only four moments are *used*. Thus, it cannot be expected to perform as well as more detailed analyses, which better reflect the specific nonlinearity in special cases. We thus compare the Hermite model here to some such special-case results: asymptotic extreme estimates of the second-order sum- or difference-frequency contribution (Næss, 1989; Næss, 1992).

RESPONSE MOMENTS: THEORY VS. SIMULATION

We first consider the statistical moments of the response, which are needed in the Hermite model. The theoretical moment analysis is first described. Because it contains no approximations, agreement with simulation should be virtually perfect. We show here how simulated moments may be affected by statistical uncertainty, however, due to histories of limited length. These results may be of interest in analyzing limited-duration model tests as well. We also consider the effects of different interpolation schemes, to simulate histories from the relatively coarse frequency mesh along which QTFs are commonly available.

For analysis or simulation, the wave elevation $\eta(t)$ at the platform center is written as a discrete Fourier sum over positive frequencies ω_k :

$$\eta(t) = \sum_{k=1}^N A_k \cos(\omega_k t + \theta_k) = \text{Re} \sum_{k=1}^N A_k e^{i(\omega_k t + \theta_k)} \quad (1)$$

To randomize Eq. 1, the phases θ_k are taken to be uniformly distributed, mutually independent of each other and of the amplitudes A_k .

The analysis assumes each of the k frequency components in Eq. 1 to be Gaussian. This is consistent with assuming the amplitude A_k to have Rayleigh distribution, with mean-square value

$$E[A_k^2] = 2S_\eta(\omega_k)\Delta\omega \equiv \sigma_k^2; \quad \Delta\omega = \omega_k - \omega_{k-1} \quad (2)$$

Therefore, for consistency we use Rayleigh-distributed amplitudes A_k in our simulations. We also caution against the common use of choosing *deterministic* amplitudes, $A_k = \sigma_k$, for these second-order load and response simulations. This can give unconservative estimates; e.g., second-order rms values that are on average too small (Ude, to appear).

The output of interest, $x(t)$, may be a wave force, structural motion, tether tension, or other response quantity. In any case we refer here to $x(t)$ generically as the total “response,” comprised of first- and second-order contributions $x_1(t)$ and $x_2(t)$:

$$x_1(t) = \text{Re} \sum_{k=1}^N A_k H_1(\omega_k) e^{i(\omega_k t + \theta_k)} \quad (3)$$

$$x_2(t) = q \text{Re} \sum_{k=1}^N \sum_{l=1}^N A_k A_l [H_2^-(\omega_k, \omega_l) e^{i[(\omega_k - \omega_l)t + (\theta_k - \theta_l)]} + H_2^+(\omega_k, \omega_l) e^{i[(\omega_k + \omega_l)t + (\theta_k + \theta_l)]}] \quad (4)$$

Here the first-order transfer function H_1 reflects the result of linear theory, while the QTFs H_2^+ and H_2^- describe second-order diffraction effects, respectively, at sum and difference frequencies. The leading factor q is included to alert readers to different QTF definitions in the literature: various codes use $q=1$ (WAMIT, 1991) or $q=1/2$ (Molin and Chen, 1990).

As expressed in Eq. 4, the second-order response $x_2(t)$ involves a weighted quadratic sum of Gaussian wave processes at various frequency components. For statistical analysis, it is unfortunate that this is a “complete” quadratic combination; i.e., with contributions from all mixed terms. Analysis is greatly simplified if $x_1(t)$ and $x_2(t)$ can be expressed as linear and quadratic forms, the latter without mixed terms:

$$x_1 = \sum_{j=1}^{2N} c_j U_j; \quad x_2(t) = \sum_{j=1}^{2N} \lambda_j U_j^2(t) \quad (5)$$

in terms of standard normal processes $U_j(t)$ that are uncorrelated at common time t . Moment analysis then requires three basic steps:

1. We first find the coefficients λ_j in Eq. 5 by solving the eigenvalue problem

$$\mathbf{\Gamma} \boldsymbol{\phi}_j = \lambda_j \boldsymbol{\phi}_j; \quad j = 1, \dots, 2N \quad (6)$$

Here the $2N \times 2N$ matrix, $\mathbf{\Gamma}$, is defined as

$$\mathbf{\Gamma} = \begin{bmatrix} \mathbf{D} & \mathbf{S} \\ \mathbf{S}^* & \mathbf{D}^* \end{bmatrix} \quad (7)$$

in terms of the $N \times N$ submatrices, \mathbf{D} and \mathbf{S} , of difference- and sum-frequency QTFs:

$$D_{kl} = \frac{q}{2} \sigma_k \sigma_l H_2^-(\omega_k, \omega_l); \quad S_{kl} = \frac{q}{2} \sigma_k \sigma_l H_2^+(\omega_k, \omega_l) \quad (8)$$

2. Once the eigenvectors $\boldsymbol{\phi}_j$ in Eq. 6 are found and normalized to have unit length, the coefficients c_j in Eq. 5 are evaluated as

$$c_j = \boldsymbol{\phi}_j^H \mathbf{h}_1 \quad (9)$$

Here \mathbf{h}_1 is a vector of first-order transfer function values (Appendix 1), and the superscript “H” denotes the Hermitian (complex conjugate) transpose. Note that while the eigenvalues

λ_j are always real, the vectors ϕ_j are typically complex. However, they have been normalized to have unit length ($\phi_j^H \phi_j = 1$), and can also be rotated so that c_j in Eq. 9 is real. Equivalently, we may first evaluate c_j from Eq. 9 and then, if the result is complex, rotate it to yield a real number. Thus, we may take c_j in Eq. 5 to be the complex magnitude $|c_j|$ of the result in Eq. 9.

3. Once c_i and λ_i are found, the moments of $x(t)$ follow directly (Næss, 1987; Winterstein and Marthinsen, 1992):

$$m_x = \sum_{j=1}^{2N} \lambda_j; \quad \sigma_x^2 = \sum_{j=1}^{2N} c_j^2 + 2\lambda_j^2 \quad (10)$$

$$\alpha_{3x} = E[(x - m_x)^3]/\sigma_x^3 = \sum_{j=1}^{2N} (6c_j^2 \lambda_j + 8\lambda_j^3)/\sigma_x^3 \quad (11)$$

$$\alpha_{4x} = E[(x - m_x)^4]/\sigma_x^4 = 3 + \sum_{j=1}^{2N} 48\lambda_j^2 (c_j^2 + \lambda_j^2)/\sigma_x^4 \quad (12)$$

If only the second-order response, x_2 , is of interest, its moments are found from setting $c_j=0$ in these results, reducing each to a single-term summation.

Appendix 1 gives the theoretical background for this procedure. Its derivation is generally traced to the electrical engineering literature (Kac and Siegert, 1947). Here, we merely note that this analysis is somewhat analogous to statistical problems such as principal components and factor analysis (Morrison, 1976). In our context, we seek marginally independent contributions (the U_j in Eq. 5) and their weights (here, the λ_j) that “best explain” the total variance of x_2 . For example, retaining only the largest eigenvalue λ_j (in absolute value) is analogous to keeping the single dominant “factor” in such analyses. Notably, this single dominant eigenvalue is found to asymptotically govern response behavior at high levels (Næss, 1989; Næss, 1992).

Numerical Results

All numerical results here use first- and second-order wave forces estimated by WAMIT (WAMIT, 1991) for the Snorre TLP. The hull has four circular columns of 25 m. diameters at 76 m. center-to-center distance, and four square pontoons with 11.3 m. sides and 2.5 m. corner radii. A coupled linear 6DOF model is used to find corresponding transfer functions for motions and tether tensions (Marthinsen and Winterstein, 1992). We consider here head seas and long-crested waves, and thus retain only the heave, pitch, and surge degrees of freedom. Including added mass effects, the natural periods are taken to be $T_n=2.3$ s in heave, 2.5s in pitch, and 83s in surge. The damping ratio in both heave and pitch is taken as $\zeta=.005$. Damping in surge is seastate-dependent; here we adopt the surge damping $\zeta=0.10$ for an extreme seastate (significant wave height $H_s=14.5$ m). Finally, all cases use a JONSWAP wave spectrum with $\gamma=3.3$.

Note that for this platform, pitch has a greater effect on tether tension than heave. We may thus expect largest springing effects when the spectral peak spectral period T_p is twice the pitch period. We therefore consider a seastate with $T_p=5$ s and $H_s=2$ m. Applying Eqs. 10 and 12 to the tether tension $x(t)$, we find

$$H_s = 2\text{m}, \quad T_p = 5\text{s}; \quad \alpha_{4,x_2} = 4.65, \quad \sigma_{x_2}/\sigma_{x_t} = .95 \quad (13)$$

Due to symmetry in the springing case, the mean and skewness of $x(t)$ are zero. These results use a regular grid of $N=200$ frequencies in Eqs. 3–4, between $\omega_{min}=0.3$ and $\omega_{max}=3.0$ rad/s. These

have been interpolated from sum-frequency WAMIT results at 218 regularly spaced (ω_1, ω_2) pairs, lying on lines between $\omega_1 + \omega_2 = 2.2$ and 2.8 rad/s.

Because 95% of the tether tension rms is due to the second-order response $x_2(t)$, it suffices to verify our predictions of second-order rms σ_{x_2} and kurtosis α_{4,x_2} . Toward this end, a number of statistically equivalent simulations were performed. Each contained $N_{pts}=4096$ points at time spacing $dt=0.2s$, producing a 13.7min segment. Note that a second interpolation of QTF values is necessary: from the $N=200$ frequencies for moment calculations to $N=4096$ regularly spaced frequencies (starting at zero) for each simulated segment. Figures 1 and 2 show results for 2 interpolations: (1) linear interpolation in real and imaginary parts, and (2) retention of the original grid, assigning each point in the fine grid the nearest neighboring QTF value from the original grid.

Interpolation (2) most faithfully preserves the QTFs used in moment prediction, and both σ and α_4 show good agreement with simulation. Note, however, the sensitivity to interpolation: linear interpolation (at this already fine mesh level) alters both σ and α_4 by about 6% in this case. One may expect greater sensitivity to the original interpolation used to generate the 200-frequency mesh from the raw WAMIT output. These issues of mesh selection, sensitivity and interpolation are topics of ongoing study.

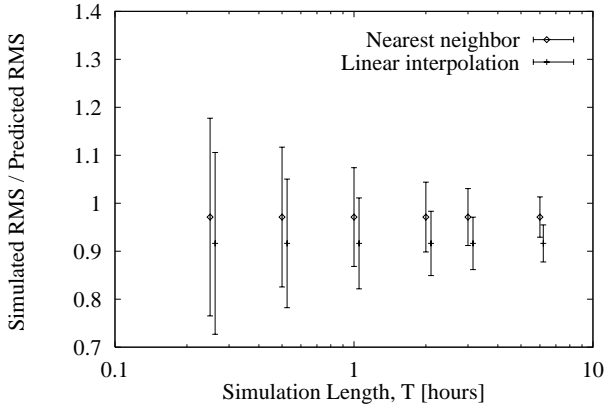


Figure 1: RMS of second-order tether tension; $H_s=2m$, $T_p=5s$.

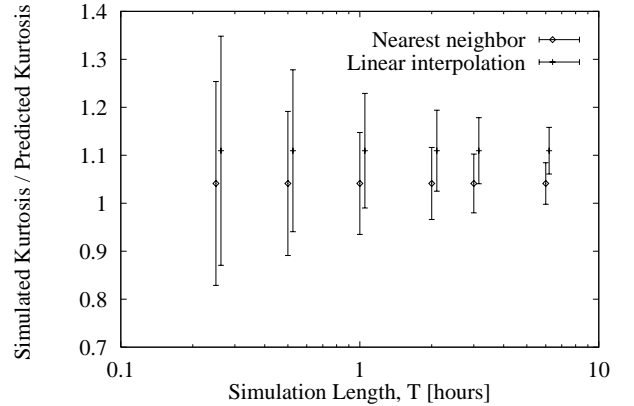


Figure 2: Kurtosis of second-order tether tension; $H_s=2m$, $T_p=5s$.

Figures 1 and 2 also show the uncertainty (standard deviation) to be expected when these moments are estimated from a limited duration time history. For a 1-hour springing history, for example, we find RMS values to have a coefficient of variation (COV=ratio of standard deviation to average) of about 10%. The kurtosis α_4 has similar COV. These together imply still larger scatter in 1-hour extremes.

Finally, a brief note about the role of error-bars in this paper. All error-bars show ± 1 standard deviation ranges. In all figures *except* Figures 1 and 2, the standard deviation applies to the estimate shown—if it is based on n simulations, this standard deviation will tend to decrease like $1/\sqrt{n}$. In the special case of Figures 1 and 2, however, the error bars are intended to apply not to our best estimate (given all simulations) but rather to the uncertainty due to a *single* simulation, with the duration shown. In this way they are intended to be suggestive of the uncertainty in a single model test result.

TETHER FATIGUE: THEORY VS. SIMULATION

Given the response moments from the preceding section, the Hermite model directly provides estimates of fatigue and extremes. The underlying premise is that the response $x(t)$ of interest is related to a standard normal process $u(t)$ by a cubic transformation:

$$x = g(u) = m_x + \kappa\sigma_x[u + c_3(u^2 - 1) + c_4(u^3 - 3u)]; \quad \kappa = [1 + 2c_3^2 + 6c_4^2]^{-1/2} \quad (14)$$

in terms of the response mean, m_x , standard deviation σ_x , and unitless coefficients c_3 and c_4 described below. While the time argument t is omitted for brevity, Eq. 14 should be understood as an assumed relation that holds at each point in time. Thus, we assume the actual non-Gaussian history can be transformed into a Gaussian history by applying a (nonlinear) distortion of the vertical, response axis. Note also that the standard normal process u here is intended to model the entire response, after cubic distortion, and is not related to the separate Gaussian contributions U_j in Eq. 5.

The coefficients c_3 and c_4 are chosen to reflect the response skewness, α_3 , and kurtosis, α_4 . Earliest versions of this model (Winterstein, 1985) assumed small nonlinearity, for which

$$c_3 \approx \alpha_3/6; \quad c_4 \approx (\alpha_4 - 3)/24 \quad (15)$$

Subsequent results (Winterstein, 1988) have used more accurate approximations. Here we propose new expressions for c_3 and c_4 , fit to “optimal results” that minimize lack-of-fit errors in α_3 and α_4 :

$$c_3 = \frac{\alpha_3}{6} \left[\frac{1 - .015|\alpha_3| + .3\alpha_3^2}{1 + 0.2(\alpha_4 - 3)} \right] \quad (16)$$

$$c_4 = c_{40} \left[1 - \frac{1.43\alpha_3^2}{\alpha_4 - 3} \right]^{1-0.1\alpha_4^{0.8}}; \quad c_{40} = \frac{[1 + 1.25(\alpha_4 - 3)]^{1/3} - 1}{10} \quad (17)$$

These results are intended to apply for $3 < \alpha_4 < 15$; $0 \leq \alpha_3^2 < 2(\alpha_4 - 3)/3$, which should include most cases of practical interest. Note that for small nonlinearities, Eqs. 16 and 17 are consistent with Eq. 15. Note also that for symmetric responses (e.g., springing), $\alpha_3=c_3=0$ and $c_4=c_{40}$.

Stochastic Fatigue Accumulation

With a Miner’s law approach, we assume a tether stress cycle with stress range S causes fatigue damage cS^m . The coefficients c and m are material properties; typical m values for offshore components range from $m=3$ to 5. If the tether stress process $x(t)$ is narrow-band Gaussian, S has Rayleigh distribution. The mean damage rate per unit time is then (e.g., Lin, 1976):

$$D_G = c\nu_0(2\sqrt{2}\sigma_x)^m(m/2)! \quad (18)$$

in terms of the standard deviation, σ_x , and mean-level upcrossing rate, ν_0 , of $x(t)$. With the skewness α_3 and kurtosis α_4 of $x(t)$, the Hermite model (Winterstein, 1988) gives the fatigue correction factor:

$$D = D_G \cdot \gamma; \quad \gamma = \frac{(\sqrt{\pi}\kappa)^m(mp)!}{(2p!)^m(m/2)!}; \quad \frac{(2p)!}{p!^2} = \frac{4}{\pi}(1 + 2c_4 + 9c_4^2) \quad (19)$$

in which c_4 is given by Eq. 17. The basis for this result is that both peaks and troughs should transform by the same g -function in Eq. 14 as the rest of the process, $x(t)$. One can therefore

transform peaks and troughs, each with Rayleigh distributions in the narrow-band normal case, and estimate the resulting range moment S^m . Eq. 19 results from doing this computation for $m=1$ and 2 only; a Weibull distribution (with shape parameter p) is then fit to S to estimate its higher moments.

This last result in Eq. 19 defines p implicitly, in terms of c_4 . In the Gaussian case, because $\alpha_3=0$ and $\alpha_4=3$ we find that $c_3=c_4=0$ and hence $p=1/2$ and $\gamma=1$. For general non-Gaussian cases, γ increases with m and α_4 , as nonlinear effects produce larger stress ranges and greater damage. Similar corrections may be derived when fatigue is caused by the tensile stress range only, as in crack growth.

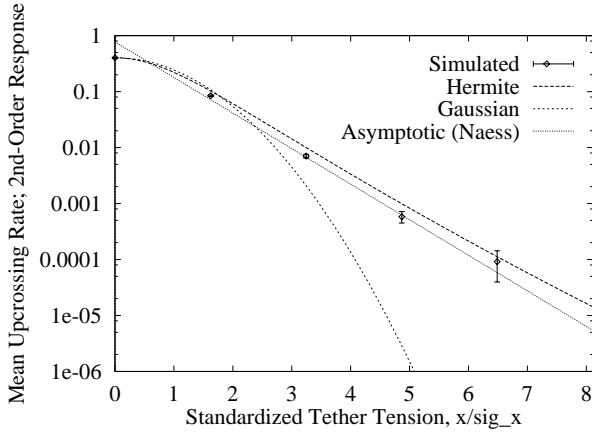


Figure 3: Upcrossing rate of tether tension; $H_s=2\text{m}$, $T_p=5\text{s}$.

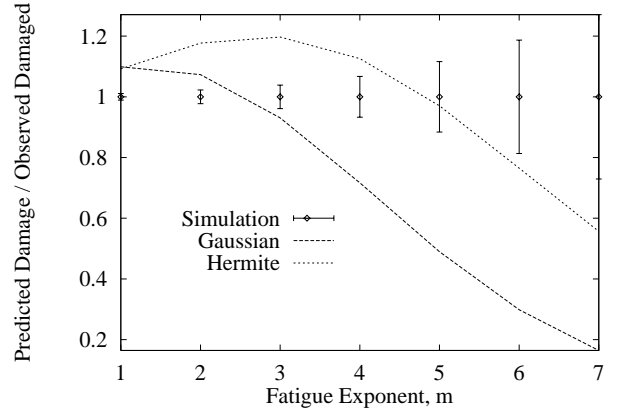


Figure 4: Fatigue damage rate for tether tension; $H_s=2\text{m}$, $T_p=5\text{s}$.

Numerical Results

We first return to the springing seastate considered earlier (Eq. 13). Because it is dominant in this case, we consider the second-order response only. Figure 3 first considers the mean rate, $\nu_x(x)$, at which the tether tension process crosses level r from below. The Hermite estimate of $\nu_x(x)$ is

$$\nu_x(x) = \nu_0 \exp(-u^2/2) \quad (20)$$

in which x and u are related through Eq. 14. For given x , the corresponding u can be found by inverting this cubic equation (Winterstein, 1988). For our purposes it is more convenient to vary u explicitly and show, as in Figure 3, the relation between x (from Eq. 14) and $\nu_0 \exp(-u^2/2)$.

Figure 3 shows that the Hermite estimate of $\nu_x(x)$ is accurate throughout a wide range of thresholds x . As expected, the Gaussian model underestimates upcrossing rates, due to its neglect of nonlinear effects that inflate the distribution tails. Also shown is an asymptotic, high-threshold estimate of $\nu_x(x)$ (Næss, 1992; Eqs. 20–21). It is more accurate than the Hermite model at all but the lowest levels—which is to be expected because it uses more than four-moment response information. The accuracy of the Hermite model appears reasonable, however, given its level of information.

Figure 4 shows the resulting fatigue damage caused by the second-order tether tension response. Simulation results use conventional rainflow counting procedures. The Gaussian estimate makes two potentially offsetting errors: it unconservatively neglects nonlinear effects, and conservatively

ignores bandwidth effects on rainflow counting. The effect of nonlinearity becomes dominant for larger fatigue exponents m ; e.g., if $m=5$ the Gaussian model predicts only half of the observed fatigue damage. The Hermite model seeks to include nonlinear effects but not bandwidth. This results in its conservative errors (of less than 20%) for $m \leq 5$. For larger m values it too is low, due to the approximate Weibull model in Eq. 19 fit to the first two moments only. More refined calculations, using the Hermite upcrossing rate in Eq. 20, lead to a systematically conservative damage estimate at all m values shown. The Hermite results shown may be sufficiently accurate, however, for the practical range of m values between 3 and 5.

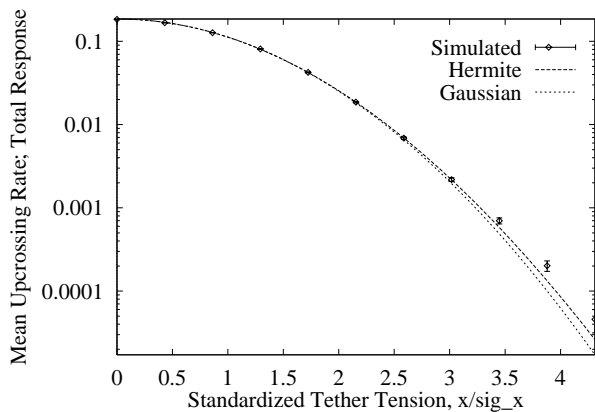


Figure 5: Upcrossing rate of tether tension; $H_s=3\text{m}$, $T_p=8\text{s}$.

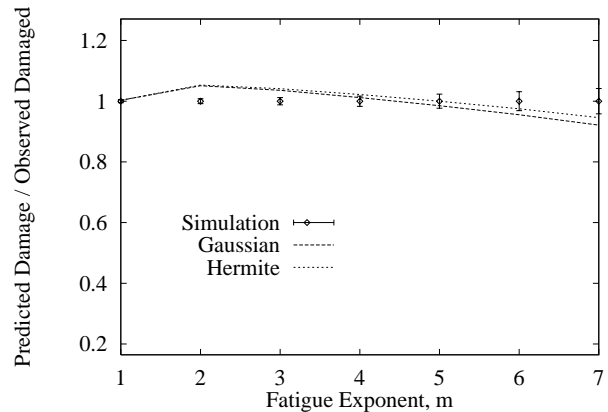


Figure 6: Fatigue damage rate for tether tension; $H_s=3\text{m}$, $T_p=8\text{s}$.

We have focused on the $T_p=5\text{s}$ seastate here to best test our ability to model second-order springing effects on fatigue. The overall damage rate will ultimately be a weighted average over all such seastates; significant contributions may also be found near $T_p=8\text{s}$, for example, if it lies near the mode of the H_s-T_p scattergram (Winterstein et al, 1994). Figure 5 shows upcrossing rate estimates for the (total) tether tension response in such a seastate, and Figure 6 the resulting fatigue damage. Here non-Gaussian effects are far smaller, and both the Gaussian and Hermite models are quite accurate.

Indeed, Figures 4 and 6 suggest that for this TLP model, non-Gaussian effects on fatigue are relatively mild. This is consistent with a more complete analysis over the entire scattergram (Winterstein et al, 1994). This reference shows, however, that far greater errors are incurred if second-order effects are completely neglected. The relatively accurate Gaussian results in Figures 4 and 6 require that we at least estimate the correct RMS level, including second-order effects.

EXTREME RESPONSE: THEORY VS. SIMULATION

Finally, we consider an example of estimating extreme deck surge in a severe seastate. The most conventional analysis of extremes is based on two assumptions: (1) the underlying process is Gaussian; and (2) crossings of high levels of practical interest occur independently. Assumption (2) will typically be conservative, as it ignores the tendency of crossings of resonant response to cluster in time. In contrast, assumption (1) will generally be unconservative for extreme

cases of interest (as in the previous fatigue examples). We therefore consider two estimates of non-Gaussian extremes here: one that retains the assumption of independent crossings, which is hoped to remain conservative, and a second that seeks to include clustering effects.

Extreme Estimates Ignoring Clustering

Assuming upcrossings to occur in Poisson fashion, the maximum response $Y = \max[x(t); 0 \leq t \leq T]$ is estimated to be

$$F_Y(y) = \exp[-\nu_x(y)T] = \exp[-Ne^{-y^2/(2\sigma_x^2)}]; \quad N = \nu_0 T \quad (21)$$

The latter result is specialized to the case of a mean-zero Gaussian response process $x(t)$. Note the use of the symbol y here to denote the maximum response, while x continues to refer to the stationary response at an arbitrary point in time.

Interest often lies not only in the distribution function $F_Y(y)$ at given y , but also in representative Y values such as its mean, median, or mode. Eq. 21 can be used directly for these purposes; e.g., the median value is found to be $\sigma_x \sqrt{2 \ln(1.44N)}$. The mean, however, requires numerical integration of Eq. 21.

It has therefore become common to introduce an additional approximation into Eq. 21. This can be done by considering a standard Gumbel variable Z . By equating its distribution function, $\exp(-e^{-z})$, to Eq. 21, we find the following relation between Z and Y :

$$Z = \frac{Y^2}{2\sigma_x^2} - \ln N \quad (22)$$

The approximation comes in replacing this exact result with an approximate linear relation:

$$Z = z_0 + z'_0 \cdot (Y - y_0) \quad (23)$$

Here y_0 is the response level about which Eq. 22 is linearized, with value $z_0 = Z(y_0)$ and slope $z'_0 = Z'(y_0)$ found from the true nonlinear relation. The benefit of Eq. 23 is that due to its linearity, substituting the mean of Z (.577) yields the corresponding mean of Y :

$$m_Y = y_0 + \frac{.577 - z_0}{z'_0} \quad (24)$$

In particular, when it is linearized around $y_0 = \sigma_x \sqrt{2 \ln N}$, Eq. 22 yields the value $z_0 = 0$ and slope $z'_0 = \sqrt{2 \ln N} / \sigma_x$, so that Eq. 24 returns the well-known formula for mean extremes (e.g., Davenport, 1964):

$$m_Y = \sigma_x \left[\sqrt{2 \ln N} + \frac{.577}{\sqrt{2 \ln N}} \right] \quad (25)$$

Note that the linearized form can also be used to estimate the median and mode of Y , replacing the mean of Z (.577 in Eq. 25) by its corresponding median or mode (.367 and 0, respectively).

The simplicity of the Hermite model is that the g -function in Eq. 14 applies at all points in time, and in particular, to the extremes of the process. Thus, once the coefficients c_3 and c_4 have been estimated from Eqs. 16–17, the mean maximum of the non-Gaussian response can be estimated as

$$m_Y = E[\max[x(t)]] = g(m_U) \quad (26)$$

Here m_U is the corresponding mean maximum of the underlying Gaussian response. This can be estimated from Eq. 25 with $\sigma_x=1$.

Extreme Estimates Including Clustering

Most analyses of clustering effects consider extremes of Gaussian processes. Such results commonly introduce a correction factor, $p(y)$, on the rate $\nu_x(y)$ in Eq. 21:

$$F_Y(y) = \exp[-\nu_x(y)p(y)T] = \exp[-Np(y)e^{-y^2/(2\sigma_x^2)}]; \quad N = \nu_0 T \quad (27)$$

Physically, we may interpret $p(y)$ as the fraction of upcrossings that can be considered to occur independently—or equivalently, $\nu_x(y)p(y)$ is the reduced rate of independent crossings once the additional crossings per cluster have been removed.

Various estimates of $p(y)$ can be found in the literature. One of the simplest (Vanmarcke, 1975) is an exponential form, based on the bandwidth parameter $\delta = \sqrt{1 - \lambda_1^2/(\lambda_0\lambda_2)}$:

$$p(y) = 1 - \exp(-Cy/\sigma_x); \quad C = \sqrt{2\pi}\delta \approx \sqrt{8\zeta} \quad (28)$$

The latter form applies to a lightly damped oscillator, with damping ratio ζ . Eq. 28 is based on direct theoretical comparison of the process $x(t)$ and its envelope $s(t)$; indeed, $p(y)$ is given by $1 - \exp(-\nu_s(y)/\nu_x(y))$. In view of its theoretical background we retain it here; comparison with some Gaussian simulations suggests that it may somewhat underestimate clustering (Vanmarcke, 1975). We may alternatively view C as an empirical parameter to be fit, for example, as a function of damping ζ .

Given this choice of $p(y)$ —or any other from the literature—we may again derive a corresponding estimate of the mean extreme m_Y . Replacing N by $Np(y)$ in Eq. 22, analogous linearization about $y_0 = \sigma_x\sqrt{2\ln N}$ now gives

$$m_Y = \sigma_x \left[\sqrt{2\ln N} + \frac{.577 + \ln p_0}{\sqrt{2\ln N} - C(1 - p_0)/p_0} \right]; \quad p_0 = 1 - \exp(-C\sqrt{2\ln N}) \quad (29)$$

This result is believed original, although it is entirely consistent with conventional first-passage approaches and approximations. As expected, it generally yields a smaller mean value than Eq. 25 which ignores clustering. As N grows, however, $p_0 \rightarrow 1$ and the two results coincide. Finally, the Hermite estimate in Eq. 26 can again be applied to reflect non-Gaussian effects; m_U in that result should now be evaluated from Eq. 29 (with $\sigma_x=1$) to include clustering effects.

Numerical Results

We consider the surge response in a relatively severe seastate: $H_s=14.5\text{m}$ and $T_p=15\text{s}$. Figure 7 show the mean upcrossing rate for the second-order contribution to surge. As in earlier sum-frequency cases, the Hermite upcrossing rates agree well with more detailed, problem-specific asymptotic results in this second-order case (Næss, 1989, Eq. 11). This agreement is maintained for the total response (Figure 8), for which fewer exact results are available.

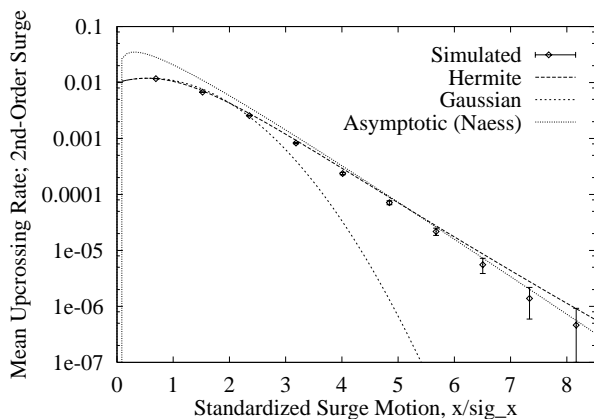


Figure 7: Upcrossing rate of second-order surge; $H_s=14.5\text{m}$, $T_p=15\text{s}$.

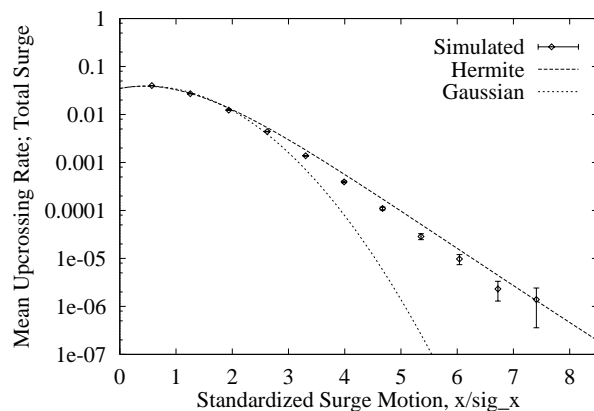


Figure 8: Upcrossing rate of total surge; $H_s=14.5\text{m}$, $T_p=15\text{s}$.

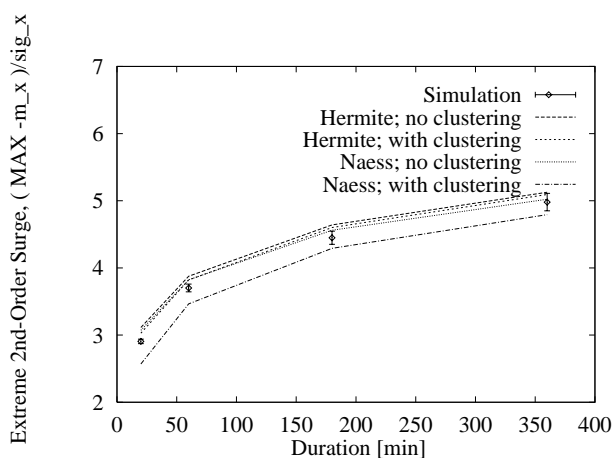


Figure 9: Average extreme second-order surge; $H_s=14.5\text{m}$, $T_p=15\text{s}$.

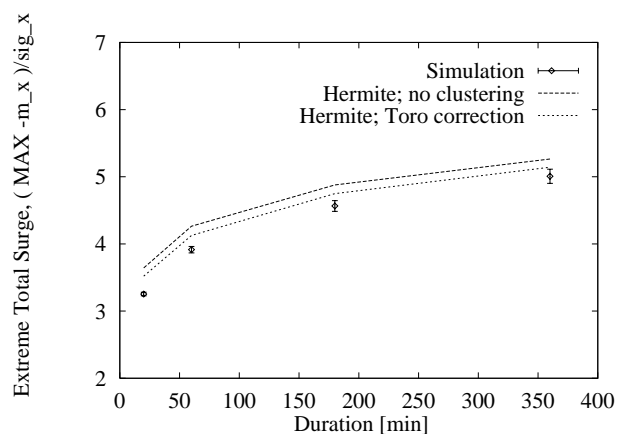


Figure 10: Average extreme total surge; $H_s=14.5\text{m}$, $T_p=15\text{s}$.

Finally, Figures 9 and 10 show corresponding estimates of average maximum sway—both second-order (Figure 9) and total (Figure 10)—over various durations. Figure 9 also shows alternate results (Næss, 1989), both without and with clustering corrections. The no-clustering result (Næss, 1989) uses Eq. 17 of this reference, while the clustering correction applies the reduction factor in Eq. 24 to the dynamic portion of Eq. 17 (with mean removed).

As expected, results that ignore clustering are found to be generally conservative. One may also expect the no-clustering limit to be more accurate for longer-duration seastates; the figures tend to reflect this trend as well. The clustering corrections in the Hermite model in Figure 9 apply the Vanmarcke correction (Eq. 28), and in Figure 10 apply a more detailed correction appropriate for bimodal response spectra (Toro and Cornell, 1986). Both appear somewhat conservative; this may be due in part to the underestimation of clustering in the original Vanmarcke correction, which underlies both results. Nonetheless, accuracy here may well be sufficient for practical purposes.

CONCLUSIONS

- A method has been shown to estimate both extremes and fatigue associated with second-order loads and responses. Based on only four marginal moments and average frequency (Eq. 14), it can be applied to an arbitrary second-order model: sum- plus difference-frequency, first- plus second-order response.
- Given its limited information, the proposed Hermite model shows good agreement with more detailed, problem-specific results for special cases; e.g., asymptotic upcrossing rate of second-order sum- or difference frequency contributions. This is shown by Figures 3 and 5 for sum-frequency cases, and by Figure 7 for difference-frequency response. It also provides accurate crossing rates for the total (first- plus second-order) response—e.g., Figures 5 and 8—where exact results are less often available.
- In its simplest form the Hermite model neglects bandwidth effects, effectively assuming a rather narrow-band response. From experience with linear Gaussian responses, this assumption would be expected to produce conservative estimates of both extremes and rainflow-counted fatigue. This conservatism is indeed generally found here, both for fatigue (with $m \leq 5$ in Figures 4 and 6) and extremes (Figures 9 and 10). In the case of extremes, a clustering correction is introduced here to reduce this conservatism.
- For this TLP model, non-Gaussian effects on fatigue are found to be relatively mild. This is true even in springing seastates (Figure 4), and especially as we move to other, more frequent seastates (Figure 6). Note, however, that far greater errors may be incurred if second-order effects are completely neglected (Winterstein et al, 1994). The relatively accurate Gaussian results in Figures 4 and 6 require that we at least estimate the correct RMS level, including second-order effects.

Acknowledgements.

This work has been primarily supported by the Reliability of Marine Structures (RMS) program of Stanford University. The authors gratefully acknowledge the ongoing intellectual and financial support of its sponsors: Amoco, Chevron, Conoco, Det Norske Veritas (DNV), Exxon, Norsk Hydro, Saga, Shell, Statoil, and Texaco.

REFERENCES

- Davenport, A.G. (1964). Note on the distribution of the largest value of a random function with application in gust loading. *Proc., Inst. of Civil Engineers London*, **28**, 187–196.
- Kac, M. and A.J.F. Siebert (1947). On the theory of noise in radio receivers with square law detectors. *J. Appl. Phys.*, **18**, 383–400.
- Langley, R.S. and S. McWilliam (1993). A statistical analysis of first and second order vessel motions induced by waves and wind gusts. *Appl. Ocean Res.*, **15**, 13–23.
- Lin, Y.K. (1976). *Probabilistic theory of structural dynamics*, Robert E. Krieger Publishing Co., Huntington, New York.
- Marthinsen, T. and S.R. Winterstein (1992). *Second-order load and response statistics for tension-leg platforms*, Rept. RMS-9, Rel. Marine Struc. Prog., Stanford University.

- Molin, B. and X.B. Chen (1990). *Calculation of second-order sum-frequency loads on TLP hulls*, Institute Français du Petrole Report.
- Morrison, D.F. (1976). *Multivariate statistical methods*, McGraw-Hill, New York.
- Næss, A. (1987). Response statistics of non-linear, second-order transformations to Gaussian loads. *J. Sound Vib.*, **15**(1), 103–127.
- Næss, A. (1989). Effects of correlation on extreme slow-drift response. *Proc., 8th Intl. Offshore Mech. Arctic Eng. Conf.*, ASME, 465–474.
- Næss, A. (1992). Prediction of extremes related to the second-order sum-frequency response of a tlp. *Proc., 2nd Intl. Offshore Polar Eng. Conf.*, ISOPE, 436–443.
- Stansberg, C.T. (1991). A simple emthod for estimation of extreme values of non-Gaussian slow-drift responses. *Proc., 1st Intl. Offshore Polar Eng. Conf.*, ISOPE, 436–443.
- Toro, G.R. and C.A. Cornell (1986). Extremes of gaussian processes with bimodal spectra. *J. Engrg. Mech.*, ASCE, **112**(5), 465–484.
- Ude, T.C. (to appear). *Identification and statistical analysis of second-order wave loads and motions*, Ph.D. thesis, Civil Eng. Dept., Stanford University.
- Vanmarcke, E.H. (1975). On the distribution of the first-passage time for nonmal stationary random processes. *J. Appl. Mech.*, ASME, **42**, 215–220.
- WAMIT, 4.0 (1991). *WAMIT: A radiation-diffraction panel program for wave-body interactions*, Users Manual, Ocean Eng. Dept., MIT.
- Winterstein, S.R. (1985). Nonnormal responses and fatigue damage. *J. Engrg. Mech.*, ASCE, **111**(10), 1291–1295.
- Winterstein, S.R. (1988). Nonlinear vibration models for extremes and fatigue. *J. Engrg. Mech.*, ASCE, **114**(10), 1772–1790.
- Winterstein, S.R. and T. Marthinsen (1991). Nonlinear effects on TLP springing response and reliability. *Computational Stochastic Mechanics: Proc. 1st Intl. Conf.*, ed. P.D. Spanos and C.A. Brebbia, Elsevier, 765–776.
- Winterstein, S.R. and T. Marthinsen (1992). *TLP springing response: reliability against extremes and fatigue*, Rept. RMS–10, Rel. Marine Struc. Prog., Stanford University.
- Winterstein, S.R., T.C. Ude, and T. Marthinsen (1994). Volterra models of ocean structures: extreme and fatigue reliability. *J. Engrg. Mech.*, ASCE, **120**(6), 1369–1385.

APPENDIX 1: EIGENVALUE ANALYSIS FOR SUM AND DIFFERENCE FREQUENCY RESPONSE

Here we provide additional details behind the development of Eq. 5. To do this, we first define a standardized Gaussian vector \mathbf{z} :

$$\mathbf{z} = \begin{bmatrix} \mathbf{z}_+^* \\ \mathbf{z}_+ \end{bmatrix}; \quad \mathbf{z}_+ = \begin{bmatrix} z_1 \\ \vdots \\ z_N \end{bmatrix} \quad (30)$$

in which z_k is defined as

$$z_k = \frac{A_k e^{i(\omega_k t + \theta_k)}}{\sigma_k} \quad (31)$$

in terms of the quantity σ_k from Eq. 2. It is readily shown from Eq. 31 that \mathbf{z} is a standard complex Gaussian vector, with covariance matrix $\mathbf{\Sigma}_{zz} = \mathbf{I}$. Orthogonality of different frequencies ensures that $E[z_j^* z_k] = 0$ for $j \neq k$. Eq. 2 then confirms that each entry z_i has unit mean-square

amplitude:

$$E[z_k^* z_k] = E[|z_k|^2] = E\left[\frac{A_k^2}{\sigma_k^2}\right] = 1 \quad (32)$$

Standardized Transfer Function Matrix

The second-order response x_2 , as defined in Eq. 4, can then be written somewhat more concisely in terms of the z_k :

$$x_2(t) = \frac{1}{2} \text{Re} \sum_{k=1}^N \sum_{l=1}^N z_k [\sigma_k \sigma_l H_2^-(\omega_k, \omega_l)] z_l^* + z_k [\sigma_k \sigma_l H_2^+(\omega_k, \omega_l)] z_l \quad (33)$$

Still more concisely, we seek a standardized second-order transfer function matrix, $\mathbf{\Gamma}$, for which the second-order response x_2 at time t can be written in a standard quadratic form:

$$x_2 = \mathbf{z}^H \mathbf{\Gamma} \mathbf{z} \quad (34)$$

With \mathbf{z} defined as in Eq. 30, we now seek a consistent choice of $\mathbf{\Gamma}$ for which Eq. 34 is satisfied. We first assume that $\mathbf{\Gamma}$ can be expressed as in Eq. 7, in terms of the $(N \times N)$ arrays \mathbf{D} and \mathbf{S} . With \mathbf{z} from Eq. 30, the quadratic form in Eq. 34 is then

$$\begin{aligned} x_2 = \mathbf{z}^H \mathbf{\Gamma} \mathbf{z} &= [\mathbf{z}_+^T \mathbf{z}_+^{T*}] \begin{bmatrix} \mathbf{D} & \mathbf{S} \\ \mathbf{S}^* & \mathbf{D}^* \end{bmatrix} \begin{bmatrix} \mathbf{z}_+^* \\ \mathbf{z}_+ \end{bmatrix} \\ &= \mathbf{z}_+^T \mathbf{D} \mathbf{z}_+^* + \mathbf{z}_+^{T*} \mathbf{D}^* \mathbf{z}_+ + \mathbf{z}_+^T \mathbf{S} \mathbf{z}_+ + \mathbf{z}_+^{T*} \mathbf{S}^* \mathbf{z}_+^* \\ &= 2 \text{Re}[\mathbf{z}_+^T \mathbf{D} \mathbf{z}_+^* + \mathbf{z}_+^T \mathbf{S} \mathbf{z}_+] \end{aligned} \quad (35)$$

Finally, by equating Eqs. 33 and 35, the definitions of \mathbf{D} and \mathbf{S} from Eq. 8 follow directly. Note also the symmetry conditions for H_2^+ and H_2^- :

$$H_2^+(\omega_k, \omega_l) = H_2^+(\omega_l, \omega_k); \quad H_2^-(\omega_k, \omega_l) = [H_2^-(\omega_l, \omega_k)]^* \quad (36)$$

These ensure that $\mathbf{\Gamma} = \mathbf{\Gamma}^H$.

Second-Order Analysis

Unlike Eq. 4, Eq. 34 expresses x_2 as a quadratic form involving *standard* normal variables. Because $\mathbf{\Gamma}$ has nonzero off-diagonal entries, mixed terms are present in this quadratic form. It remains to rotate entries of \mathbf{z} , so that these mixed terms are eliminated. Such a rotation is made possible by the eigenvalue analysis, which provides the spectral decomposition:

$$\mathbf{\Gamma} = \mathbf{\Phi} \mathbf{\Lambda} \mathbf{\Phi}^H \quad (37)$$

in which $\mathbf{\Lambda}$ is a diagonal matrix with entries λ_j , and $\mathbf{\Phi}$ is a matrix whose columns are the eigenvectors ϕ_j . (This is merely a restatement of Eq. 6, using unit-length eigenvectors so that $\mathbf{\Phi}^{-1} = \mathbf{\Phi}^H$). Combining Eqs. 34 and 37,

$$x_2 = \mathbf{u}^H \mathbf{\Lambda} \mathbf{u} = \sum_{j=1}^{2N} \lambda_j |u_j|^2; \quad \mathbf{u} = \mathbf{\Phi}^H \mathbf{z} \quad (38)$$

We use the subscript j here to denote a summation over all *eigenmodes*, as distinct from summations over all frequencies (indices k and l in the preceding). Note also that \mathbf{u} is a rotated version of \mathbf{z} , in which lengths (and covariances) are preserved:

$$\mathbf{\Sigma}_{uu} = E[\mathbf{u} \mathbf{u}^H] = \mathbf{\Phi}^H E[\mathbf{z} \mathbf{z}^H] \mathbf{\Phi} = \mathbf{\Phi}^H \mathbf{\Phi} = \mathbf{I} \quad (39)$$

In view of this standardization, $|u_j|^2$ is a standard chi-square variable. This confirms the equivalence between x_2 in Eqs. 4 and 5.

First-Order Analysis

Finally, we also confirm that x_1 in Eq. 3 can be recast into the form given by Eq. 5. We can first rewrite Eq. 3 in vector form:

$$x_1 = \mathbf{h}_1^H \mathbf{z} \quad (40)$$

in which $\mathbf{h}_1^H = [\sigma_N H_1(\omega_N) \dots \sigma_1 H_1(\omega_1) \sigma_1 H_1^*(\omega_1) \sigma_N H_1^*(\omega_N)]$ and $\mathbf{z}^H = [z_n \dots z_1 z_1^* \dots z_n^*]$. But $\mathbf{z} = \mathbf{\Phi} \mathbf{u}$, in view of the definition of \mathbf{u} in Eq. 37. Substituting this into Eq. 40,

$$x_1 = \mathbf{h}_1^H \mathbf{\Phi} \mathbf{u} = \mathbf{c}^H \mathbf{u} = \sum_{j=1}^{2N} c_j u_j \quad (41)$$

in which c_j is as given in Eq. 9.